Generalized perturbation techniques for uncertainty quantification in lead-cooled fast reactors

Generalized Perturbation Techniques for Uncertainty Quantification in Lead-Cooled Fast Reactors

Nicolò Abrate[a], Sandra Dulla[a], Piero Ravetto[a]

[a] *Politecnico di Torino, Dipartimento Energia, Corso Duca degli Abruzzi, 24 - 10129 Torino (Italy)*

Abstract

The design of innovative nuclear fission systems requires a careful evaluation of the uncertainties affecting the basic input data. Among them, nuclear data are particularly relevant, due to their dramatic energy dependence. Because of this feature and of the strong spatial heterogeneity of nuclear reactors arrangement, full-core calculations are carried out using energy collapsed and spatially homogenised constants. Nowadays, collapsing is often performed with Monte Carlo codes, which allow a discretisation-free treatment of the neutron transport equation.

The most popular method to propagate the uncertainty in the nuclear data libraries throughout the Monte Carlo transport calculation is the Generalised Perturbation Theory (GPT). However, due to its multi-group nature, GPT often blurs the continuous-energy feature of the Monte Carlo method. Therefore, in order to fully exploit its advantages, the XGPT method has been recently proposed. After discussing the main differences between these two approaches, the paper presents the application to an uncertainty quantification study on the lead-cooled fast reactor ALFRED design, performed with GPT and focused on the multi-group cross sections.

Afterwards, the two nuclides that most contribute to the overall uncertainties, i.e. Pu-239 and U-238, are considered to compare the GPT results to some XGPT calculations carried out with different multi-group energy structures. This analysis suggests that XGPT is a consistent method for uncertainty quantification in the continuous-energy Monte Carlo framework. Moreover, it can be concluded that an adequate number of low-energy groups

Email addresses: nicolo.abrate@polito.it (Nicolò Abrate), sandra.dulla@polito.it (Sandra Dulla), piero.ravetto@polito.it (Piero Ravetto)

is necessary for an accurate uncertainty evaluation in the case of a fast system.

Keywords: uncertainty propagation; sensitivity analysis; reduced-order models; GPT; XGPT; Monte Carlo; Serpent 2 code; nuclear data; lead-cooled fast reactor;

Foreword by Sandra Dulla

The year 2020 has been dubbed *annus horribilis* for reasons that are very clear to the whole society, and it is also the year when Massimo Salvatores left us. He passed away, but the correct statement is really "he left us", as the void he left in our scientific community, and our hearts, is practically irreplaceable.

In his long career, he has provided fundamental contributions in basically every reactor physics-related topic and beyond. His work on Generalized Perturbation Theory is just one example, and this paper aims at honoring his legacy with a, tiny in comparison, contribution.

A paper in this special issue written by P. Ravetto and G. Palmiotti provides a beautiful summary of Massimo's works, and we do get a glimpse on Massimo's life thanks to the obituary by G. Palmiotti and A. Gandini. All the persons who had the luck to cross paths with Massimo surely have some nice memories of the event, typically combining the scientific exchanges with the human aspects.

I do have my own memories. In September 2012 Massimo Salvatore came to Politecnico di Torino to give a PhD excellence course on "Multiphysics problems for advanced nuclear application". It was my occasion to appreciate, together with the many PhD students participating to the course, Massimo's outstanding skills as teacher, his passion for science and clear vision for the future of nuclear engineering research. I also remember a colleague from a neighboring field being almost mesmerized by Massimo's clear talking and engaging thinking, but the best memory comes from a different field. Massimo spent some time in our offices, talking to one of our PhD student at that time. She then told me she would have loved to have a grandfather as Massimo, who was taking his granddaughter to London to watch the opera. I did share that feeling.

In 2018 Massimo was giving a plenary talk at the PHYSOR conference entitled "Measuring the earth and the sky", where he was able to summarize,

in a single talk, notions related to the history and art of Mexico with reactor physics concepts. Later that night, in front of a drink, he was asked questions on the latter and, naturally, provided his enlightening physical insight. That conference was for some of us a wonderful occasion to spend some time with him, talking about travels, food and even tv series, discovering a side of him that you cannot get from his immense scientific production.

Massimo Salvatores was to me a scientific father, a title I can give to a few, exceptional figures in our scientific community. This is why, when I got the information of his condition in early March 2020, the news hit me this hard. At the same moment, my father was in hospital for the COVID infection. Of these two, unfortunately, only one managed to get out of that extremely difficult time.

My heart is half-broken for this scientific father I lost.

1. Introduction

One of the methodologies currently employed for the safety assessment of nuclear reactors is the so-called Best Estimate Plus Uncertainty (BEPU) approach, which aims at qualifying the results provided by high fidelity computational codes with an estimate of their uncertainty [1, 2]. The uncertainty affecting the calculations may be epistemic, i.e. the one related to the physico-mathematical model and its assumptions (e.g., multi-group vs. continuous-energy, diffusion vs. transport, ...), or aleatory, due to the intrinsic randomness in the phenomena observed [3].

The uncertainty in the basic nuclear data, such as cross sections or energy-angular distributions, is the combination of both contributions and it is a relevant source of the overall uncertainty associated to a best estimate calculation. More specifically, the uncertainty in the raw nuclear data affects directly the homogenised and collapsed multi-group constants, which are generated for the full-core neutronic analyses. The common approach to generate the multi-group data is using high-fidelity codes that address space, energy and angle in detail, thus providing an accurate estimate for the flux at the assembly level. The flux information is then used to collapse on energy and homogenise over space the cross sections. This step is usually carried out using deterministic codes like the ECCO-ERANOS system [4] or, more recently, using Monte Carlo codes [5]. In spite of their larger computational burden, stochastic methods allow to reduce as much as possible both the modeling and the numerical errors, because of the discretization-free treatment of the

phase space. On the other hand, due to the nature of the method, Monte Carlo calculations are affected by statistical uncertainty.

Whatever is the methodology employed to generate the multi-group constants, the nuclear data vector p uncertainty on the output vector response r of interest is usually assessed using the well-known sandwich rule [6],

$$\mathrm{var}[r] = \vec{\mathrm{S}}_p^r \mathrm{cov}[p] \vec{\mathrm{S}}_p^{r^T}, \tag{1}$$

where $\mathrm{var}[r]$ is the variance of the response, $\vec{\mathrm{S}}_p^r$ is the relative sensitivity of r with respect to a variation in the input p, and $\mathrm{cov}[p]$ is the relative covariance matrix associated to p. In spite of its first-order accuracy, eq. (1) is widely employed in nuclear engineering to propagate uncertainty in combination with Generalized Perturbation Theory (GPT), a surrogate technique based on the forward and adjoint neutron models, originally developed by L.N. Usachev and later exploited by A. Gandini and M. Salvatores [7, 8]. GPT allows to estimate the sensitivities to a large number of input parameters for many responses in a computationally efficient manner, although the information conveyed is limited to the response uncertainty.

If a richer information is coveted, e.g. the response distribution or its moments, an Uncertainty Quantification (UQ) study can be carried out with a direct sampling technique. Among the various sampling methods available, the so-called Total Monte Carlo (TMC) method [9] is one of the best candidates for UQ, since it is not subjected to the curse of dimensionality [10]. Nevertheless, this approach is extremely computationally intensive, as it scales like $1/\sqrt{N}$, where N is the number of samples.

A promising alternative to both GPT and TMC is represented by a recently developed method, the eXtended Generalised Perturbation Theory (XGPT). This algorithm, currently implemented in Serpent 2 [11, 12], is a first-order projection technique that can be employed to build approximated response distributions, working as a reduced-order version of TMC. This feature makes XGPT very interesting, especially as a fast, yet still accurate, tool to estimate the distributions of multi-group constants due to the uncertainty in the input parameters. Such a kind of uncertainty analysis is of paramount importance for a proper safety-oriented design of innovative reactors like the Gen-IV fast systems, whose behaviour is featured by a strong interplay between neutronics and thermal-hydraulics. The intrinsic multiphysics nature of such systems and the presence of uncommon nuclides with respect to currently operating reactors require the adoption of state-of-the-art techniques

for the correct propagation of the uncertainty from the nuclear data to the final output of the calculation chain, e.g. Polynomial Chaos Expansion (PCE) [13].

Polynomial Chaos Expansion is a surrogate technique that allows to propagate the uncertainty from the input data to the output of a computational model with a limited number of model executions, thanks to a clever choice of the samples. However, to exploit the full potential of this technique, the distributions for the model input parameters are necessary, even in an approximated form.

The XGPT approach may provide the missing piece for a consistent UQ from the raw nuclear data to the multiphysics full-core calculations. Therefore, this work aims to assess the possibility to generate output response distributions using XGPT, focusing on some selected multi-group constants. The first part of the paper presents a preliminary UQ study carried out on the ALFRED (Advanced Lead Fast Reactor European Demonstrator) reactor design [14], using the legacy GPT approach. Afterwards, two relevant nuclides are chosen to compare the uncertainties estimated with the GPT and XGPT methods implemented in Serpent 2, analysing the influence of the different tuning parameters, e.g. the energy grid structure. Finally, the distributions for some output responses are computed using XGPT method and conclusions on the potential of this reduced-order model are drawn.

2. Generalized perturbation methods for uncertainty quantification

This section is devoted to describe the GPT and XGPT methods, pointing out their the main features.

GPT is a legacy reactor physics approach, therefore it is available as a standard routine in most deterministic codes [4]. Since these codes discretise the energy axis with the multi-group approximation, both the sensitivity coefficients computed with GPT and the covariance matrices employed in eq. (1) are evaluated on multi-group structures. This fact has induced the nuclear data evaluators to develop methods and tools [15] to process the covariance matrices over relatively coarse energy structures (usually no more than a thousand groups). In spite of this approximation, GPT has been applied successfully for sensitivity and uncertainty analyses in reactor physics and engineering applications since the 70's, thanks especially to the contributions given by A. Gandini and M. Salvatores. Due to its popularity, GPT has

also been implemented in various continuous-energy Monte Carlo codes, like MCNP [16] and Serpent 2. Nevertheless, in spite of the absence of any energy approximation, also Monte Carlo GPT provides group-wise sensitivities, since the statistical error increases if the tally bin width is reduced.

In order to overcome this Monte Carlo GPT limitation, the XGPT method has been proposed [11]. The main idea of this approach is to compute the sensitivities by means of scalar products on basis functions extracted from the covariance matrices. Since the scalar products involve integration over the energy, the XGPT coefficients are less prone to statistical issues, potentially allowing continuous-energy evaluations.

In addition to the improvements in the calculation of the sensitivity coefficients, XGPT also permits the adoption of "high-resolution" covariance matrices, i.e. evaluated on a fine energy grid. Nevertheless, due to the historical development of multi-group codes, it is still not possible, nowadays, to process the Evaluated Nuclear Data Files (ENDF) tapes into a continuous-energy format. The only relevant exception, to the authors' knowledge, consists in extracting the sample covariance matrices from a set of continuous-energy perturbed ENDF tapes generated with the T6 package [17, 18, 19], as done in [11].

Figure 1 shows some examples of correlation matrices for Pu-239 and U-238 data, taken from the ENDF/B-VIII.0 library [20] and evaluated on different energy grids with the ERRORR module of NJOY [15]. It is interesting to notice that the impact of the energy grids is straightforward for Pu-239 and less evident for U-238, as it will be examined in more detail later.

The following subsection is devoted to highlight the main differences between the sensitivity evaluation by GPT and XGPT methods.

2.1. Evaluation of sensitivity coefficients

For a given physical system, the first-order relative sensitivity of a certain response R of the system to a certain physical parameter P is defined as:

$$S_P^R = \frac{\partial R/R}{\partial P/P} = \frac{P}{R}\frac{\partial R}{\partial P}. \tag{2}$$

In this paper, the parameter P is always assumed to be the microscopic cross section of a specific nuclide j for a certain reaction y, i.e. $\sigma_{y,j}(E)$, while the response is assumed to be the linear reaction rate ratio that defines the macroscopic cross section for reaction x, homogenised over a region of volume

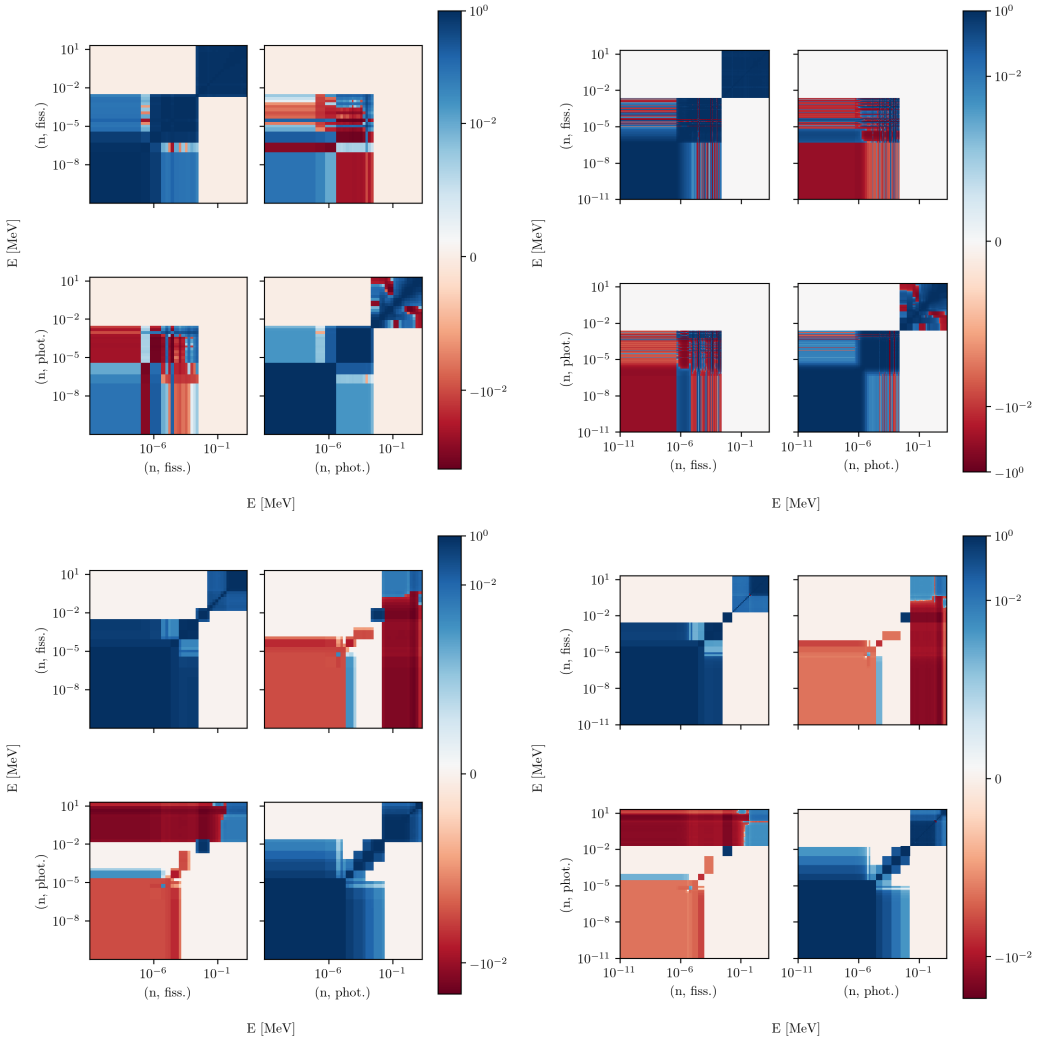

Figure 1: Correlation matrices for Pu-239 (top) and U-238 (bottom) data evaluated on ECCO-33 groups (left) and using 1500 groups (right).

V and collapsed over a energy group g,

$$R_g^x = \frac{\displaystyle\int_V d\vec{r} \int_{E_{g-1}}^{E_g} dE\ \Sigma_x(\vec{r},E)\Phi(\vec{r},E)}{\displaystyle\int_V d\vec{r} \int_{E_{g-1}}^{E_g} dE\ \Phi(\vec{r},E)} = \frac{\langle \Sigma_x|\Phi\rangle_g}{\langle 1|\Phi\rangle_g} = \frac{R_{1,g}^x[\Sigma_x,\Phi]}{R_{2,g}^x[\Phi]}, \quad (3)$$

where the notation adopted highlights the fact that the response of interest is the ratio of two functionals, $R_{1,g}^x$ and $R_{2,g}^x$. As a consequence, eq. (2) can be manipulated in order to get:

$$S_P^{R_x^g} = P\frac{R_{2,g}^x}{R_{1,g}^x}\frac{\partial}{\partial P}\left(\frac{R_{1,g}^x}{R_{2,g}^x}\right) = \frac{P}{R_{1,g}^x}\frac{\partial R_{1,g}^x}{\partial P} - \frac{P}{R_{2,g}^x}\frac{\partial R_{2,g}^x}{\partial P} = S_P^{R_{1,g}^x} - S_P^{R_{2,g}^x}. \quad (4)$$

The term $S_P^{R_{1,g}^x}$ can be expressed as the sum of two first-order functional derivatives, as:

$$S_P^{R_{1,g}^x} = \frac{P}{R_{1,g}^x}\frac{\langle \delta\Sigma_x|\Phi\rangle_g}{\delta P} + \frac{P}{R_{1,g}^x}\frac{\langle \Sigma_x|\delta\Phi\rangle_g}{\delta P} = S_{P,dir}^{R_{1,g}^x} + S_{P,ind}^{R_{1,g}^x} \quad (5)$$

that are usually referred to as the *direct* and the *indirect* terms, respectively. The direct term represents the change of the macroscopic cross section due to P, while the indirect term represents the flux change due to P. From now on, the variation symbol δ will be used in substitution of the continuous derivative.

Starting from version 2.1.31, Serpent is able to compute automatically both $S_{P,dir}^{R_{1,g}^x}$ and $S_{P,ind}^{R_{1,g}^x}$ only when the GPT routine is employed. If the XGPT mode is adopted, the user must define suitable detectors in order to estimate also the direct term.

To obtain the explicit tally definitions to be employed to estimate the direct sensitivities presented in this work, it is useful to notice that, for a heterogeneous system like the ALFRED reactor, Σ_x can be usually expressed as

$$\Sigma_x(\vec{r},E) = \sum_{i=0}^{I} N_i(\vec{r})\sigma_{x,i}(E), \quad (6)$$

where N_i is the atomic density of the i-th nuclide species. Since the analysis carried out in this paper concerns only the fissile isotopes, the atomic density

spatial distribution is a piece-wise constant,

$$N_i(\vec{r}) = \begin{cases} N_i & \forall \vec{r} \in D_1 \cup D_2 \cup ... \cup D_F \\ 0 & \text{otherwise,} \end{cases} \tag{7}$$

where D_k indicates the k-th fuel pellet volume.

Equations (6) and (7) allow to evaluate the direct term explicitly for the case $P = \sigma_{y,j}(E)$:

$$\begin{aligned} S^{R^x_{1,g}}_{P,dir}(E) &= \frac{\sigma_{y,j}(E)}{R^x_{1,g}} \frac{\langle \delta\Sigma_x | \Phi \rangle_g}{\delta\sigma_{y,j}(E)} \\ &= \frac{\sigma_{y,j}(E)}{R^x_{1,g}} \frac{1}{\delta\sigma_{y,j}(E)} \int_V d\vec{r} \int_{E_{g-1}}^{E_g} dE \ \delta\Sigma_x(\vec{r}, E)\Phi(\vec{r}, E) \\ &= \frac{\sigma_{y,j}(E)}{R^x_{1,g}} \frac{1}{\delta\sigma_{y,j}(E)} \int_V d\vec{r} \int_{E_{g-1}}^{E_g} dE \ \sum_{i=0}^{I} N_i(\vec{r})\delta\sigma_{i,x}(E)\Phi(\vec{r}, E) \\ &= \frac{\sigma_{y,j}(E)}{R^x_{1,g}} \sum_{i=0}^{I} \int_V d\vec{r} N_i(\vec{r}) \int_{E_{g-1}}^{E_g} dE \ \Phi(\vec{r}, E) \frac{\delta\sigma_{i,x}(E)}{\delta\sigma_{y,j}(E)}, \end{aligned} \tag{8}$$

The direct sensitivity coefficient vanishes if reactions x and y are independent or if the nuclide species i and j are not the same, therefore the previous equation reduces to:

$$S^{R^x_{1,g}}_{P,dir}(E) = \frac{N_j \sigma_{y,j}(E)}{R^x_{1,g}} \int_{V_F} d\vec{r}\Phi(\vec{r}, E)\delta_{xy}, \tag{9}$$

where δ_{xy} acts as the standard Kronecker operator and V_F is the total fuel volume inside the volume V considered for the homogenisation. As previously mentioned, the major difference between GPT and XGPT lies in the way the sensitivity defined in eq. (4) is scored. GPT scores group-wise sensitivities,

$$S^{R^x_g}_{P,h} = \int_{E_h}^{E_{h+1}} dE \ S^{R^x_g}_P(E), \quad \forall \ h = 1, \ldots, H, \tag{10}$$

while XGPT scores the projections of the sensitivity coefficient $S^{R^x_g}_P(E)$ on continuous-energy basis functions $b_k(E)$ extracted from the covariance ma-

trices,

$$\begin{aligned} S^{R_g^x}_{P,k} &= \int_{E_{\min}}^{E_{\max}} dE\ S^{R_g^x}_{P}(E) b_k(E) \\ &= \int_{E_{\min}}^{E_{\max}} dE\ \left(S^{R^x_{1,g}}_{P,dir}(E) + S^{R^x_{1,g}}_{P,ind}(E) - S^{R^x_{2,g}}_{P}(E) \right) b_k(E), \end{aligned} \tag{11}$$

where the integration is carried out between the minimum and maximum energies considered for the intended calculation. Since the direct effect for a collapsed cross section is only affected by perturbations occurring within its energy boundaries, it can be written in XGPT fashion as:

$$\begin{aligned} S^{R^x_{1,g}}_{P,dir,k} &= \int_{E_g}^{E_{g+1}} dE\ S^{R^x_{1,g}}_{P,dir}(E) b_k(E) \\ &= \frac{1}{R^x_{1,g}} \int_{E_g}^{E_{g+1}} dE\ N_j \sigma_{j,x}(E) b_k(E) \int_{V_F} d\vec{r} \Phi(\vec{r}, E) \\ &= \frac{1}{\langle \Sigma_x | \Phi \rangle_g} \int_{E_g}^{E_{g+1}} dE\ \Sigma_{j,x}(E) b_k(E) \int_{V_F} d\vec{r} \Phi(\vec{r}, E). \end{aligned} \tag{12}$$

While the denominator of eq. (12) can be evaluated defining a suitable tally, it is not possible to directly score the scalar product over the basis functions. To overcome this issue, the integral is evaluated *a posteriori*, scoring the reaction rate over the whole volume of interest and over the same energy grid employed to define the basis functions. In such a way, the integration can be approximated as follows:

$$\int_{E_g}^{E_{g+1}} dE\ \Sigma_{j,x}(E) \Psi(E) b_k(E) \cong \sum_{h=1}^{H} \Sigma_{j,x,h} \Psi_h b_{k,h} \Delta E_h, \tag{13}$$

where Ψ is the flux integrated over the fuel volume. All the sensitivity and tally results presented throughout the paper have been processed using the serpentTools package [21] and some in-house Python scripts. Despite the projection requires an *ad hoc* implementation in the Monte Carlo code, it is useful to observe that this procedure could be employed as an *a posteriori* step to obtain approximated projections using group-wise sensitivities evaluated on a sufficiently fine energy grid:

$$S^{R_g^x}_{P,b_k} = \int_{E_{\min}}^{E_{\max}} dE\ S^{R_x^g}_{P}(E) b_k(E) \cong \sum_{h=1}^{H} S^{R_x^g}_{P,h} b_{k,h} \Delta E_h. \tag{14}$$

This approach would not require any code modifications and could potentially disclose the possibility of using also deterministic codes to get approximated response distributions.

2.2. Determination of the basis functions

The basis functions employed in the scalar product of the sensitivity coefficients can be computed by means of the Proper Orthogonal Decomposition (POD) algorithm [22], which is a classical technique for the dimensionality reduction of a set of data.

If the set of perturbed cross sections is available, the POD can be performed computing the Singular Value Decomposition (SVD) of the snapshot matrix, i.e. the matrix whose columns are the perturbed data. These data can be sampled, for example, using the SANDY code [23] or the T6 package [19], which allows to apply continuous-energy perturbations to the ENDF files and, consequently, to obtain a continuous-energy sample covariance matrix. This approach is described in more detail in [11] and [24]. If the information available is the covariance matrix stored in the ENDF-6 files, the POD can be performed via SVD of the covariance matrix itself. This second approach, followed in this paper, allows to avoid the introduction of statistical errors and biases related to the sample covariance matrix evaluation, but limits its energy resolution.

The POD computed via SVD allows to factorise the relative covariance matrix $\mathrm{cov}[p] \in \mathbb{R}^{m\times m}$ as

$$\mathrm{cov}[p] = \hat{B}\hat{\Sigma}\hat{A}^{\intercal}, \tag{15}$$

where $\hat{B} \in \mathbb{R}^{m\times m}$ is the column-wise set of $\mathrm{cov}[p]$ left eigenvectors, $[\vec{b}_1, \vec{b}_2, \ldots, \vec{b}_m]$, $\hat{\Sigma} \in \mathbb{R}^{m\times m}$ contains $\mathrm{cov}[p]$ singular values and $\hat{A} \in \mathbb{R}^{m\times m}$ is the column-wise set of $\mathrm{cov}[p]$ right eigenvectors. In this case $\hat{A} = \hat{B}$, since $\mathrm{cov}[p]$ is square and symmetric.

The dimensionality reduction can be carried out thanks to the fact that the singular values σ_i of $\mathrm{cov}[p]$ constitute a monotonically decreasing sequence ($\sigma_1 > \sigma_2 > ... > \sigma_m$) that decays quickly. Since each eigenvalue is proportional to the information carried by the corresponding basis function, it is possible to approximate the original matrix $\mathrm{cov}[p]$ using a limited number t of eigenvectors. The value of t is often chosen looking at the value of

the POD energy, defined as

$$\mathcal{E}(t) = \frac{\sum_{k=1}^{t} \sigma_k^2}{\sum_{k=1}^{r} \sigma_k^2}. \tag{16}$$

The POD energy is equal to 1 when $t = m$. In this case, the tolerance is checked against $1 - \mathcal{E}$.

2.3. XGPT uncertainty quantification

Once the projected sensitivities $S^r_{p,b_k}\ \forall\ k = 1, ..., t$ are computed, one may compute the response variance using the sandwich formula, or use XGPT in a reduced-order fashion to approximate the response distribution. In the first case, the uncertainty is estimated starting from the continuous version of the sandwich formula [11],

$$\begin{aligned}
\text{var}[r] &= \int_{E_{\min}}^{E_{\max}} dE \int_{E_{\min}}^{E_{\max}} dE' S^r_p(E) \text{cov}[p](E, E') S^r_p(E') \\
&= \int_{E_{\min}}^{E_{\max}} dE \int_{E_{\min}}^{E_{\max}} dE' S^r_p(E) \hat{B}(E) \hat{\Sigma} \hat{B}(E')^\intercal S^r_p(E') \\
&= \left(\int_{E_{\min}}^{E_{\max}} dE\ \hat{B}(E)^\intercal S^r_p(E) \right)^\intercal \hat{\Sigma} \left(\int_{E_{\min}}^{E_{\max}} dE\ \hat{B}(E)^\intercal S^r_p(E) \right) \\
&= \vec{S}^{r\intercal}_{p,b}\ \hat{\Sigma}\ \vec{S}^r_{p,b},
\end{aligned} \tag{17}$$

where $\vec{S}^r_{p,b}$ is the column vector obtained stacking the projected sensitivities S^r_{p,b_k}. Since $\hat{\Sigma}$ is a diagonal matrix whose entries are filled with the singular values of cov[p], eq. (17) turns out to be a weighted sum of smaller and smaller contributions.

Using the same quantities, it is possible to build a first-order model to approximate the full-order model output response. Starting from eq. (2) and assuming a linear variation, the model yields:

$$\begin{aligned}
\frac{R_i - R_0}{R_0} = \vec{S}^{R\intercal}_P \frac{\vec{P}_i - \vec{P}_0}{\vec{P}_0} = \vec{S}^{R\intercal}_P \vec{X}_i = \vec{S}^{R\intercal}_P \hat{I} \vec{X}_i = \\
= \vec{S}^{R\intercal}_P \hat{B}_t \hat{B}^\intercal_t \vec{X}_i = (\hat{B}^\intercal_t \vec{S}^R_P)^\intercal \hat{B}^\intercal_t \vec{X}_i = \vec{S}^{R\intercal}_{P,b} \vec{\alpha}_i\ ,
\end{aligned} \tag{18}$$

where $\hat{B}_t$ is the truncated POD basis $\hat{B}$ and $\vec{\alpha}_i$ is the $i-$th response projection in the reduced space. Rearranging the terms, eq. (18) finally yields

$$R_i = R_0 \left(1 + \sum_{k=1}^{t} \alpha_{ik} S^R_{P,b_k} \right). \tag{19}$$

Thanks to eq. (19), the output response to an input perturbation $\vec{P}_i$ can be computed in a fully consistent way with respect to the continuous-energy Monte Carlo approach, disclosing the possibility of performing a first-order uncertainty propagation from the raw nuclear data to the output homogenised coarse-group constants.

It is important to notice that, according to the way the basis functions are computed, eq. (19) may yield different approximations to the output distribution. If the basis functions were extracted directly via SVD of the covariance matrix, they would not contain any information on the input parameter distribution. In this case, eq. (19) acts as a linear model that approximates the output distribution of an input parameter that is implicitly assumed to be normally distributed. This implies that also the output will be normally distributed as well.

On the contrary, if the basis functions were computed applying POD to the snapshot matrix [22], the basis functions would convey a richer statistical information, since they would contain also an information related to the distribution of the samples. In this last case, the model would behave as a linearized TMC approach.

3. Application to the ALFRED reactor model

The methodology previously described is now applied to a Monte Carlo model of the ALFRED reactor design. The geometry and material specifications are taken from [14] for the Lead-Cooled Fast Reactor design, developed within the European project LEADER. We consider the Beginning of Life (BoL) configuration, with all the safety and control rods withdrawn. The 3D model also includes the barrel and the external lead.

The regions considered for the spatial homogenisation of the multi-group data are reported, for the reader's convenience, in figure 2. The left sketch represents the different types of assemblies, which are discretised axially as shown in the right sketch. The multi-group constants of this reactor discretisation, collapsed over the groups described in table 1, were employed in the

framework of a benchmark between the neutronic module of the FRENETIC (Fast REactor NEutronics /Thermal-hydraulICs) code and Serpent, showing a very good agreement with respect to k_{eff} and thermal power distribution [25]. The reference thermodynamic condition considered in this paper to take into account the Doppler effect is a uniform temperature equal to 1073 K for the whole system. All the Monte Carlo calculations have been carried out using the ENDF/B-VIII.0 nuclear data library.

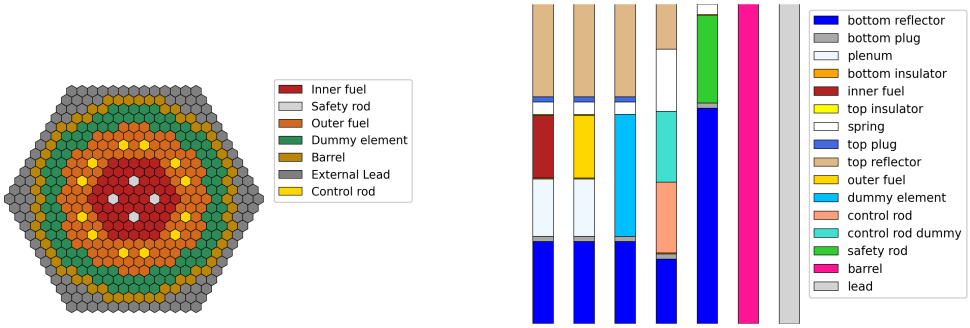

Figure 2: Radial section (left) and axial regions (right) of ALFRED 3D model, as in [25].

Table 1: Six-group energy grid adopted to perform the macroscopic cross section energy collapsing [25].

Group	Upper boundary [MeV]	Lower boundary [MeV]
1	$2.000 \cdot 10^{1}$	$1.353 \cdot 10^{0}$
2	$1.353 \cdot 10^{0}$	$1.832 \cdot 10^{-1}$
3	$1.832 \cdot 10^{-1}$	$6.738 \cdot 10^{-2}$
4	$6.738 \cdot 10^{-2}$	$9.119 \cdot 10^{-3}$
5	$9.119 \cdot 10^{-3}$	$2.000 \cdot 10^{-5}$
6	$2.000 \cdot 10^{-5}$	$1.000 \cdot 10^{-11}$

3.1. Uncertainty quantification with GPT

In this section, the results of a UQ study using the GPT approach [26] are presented and discussed. The Serpent code responses analysed in the following are the effective multiplication factor k_{eff} and the six-group fission and capture cross sections, $\Sigma_{f,g}$ and $\Sigma_{c,g}$, homogenised over the inner and outer fuel regions of ALFRED. The perturbations considered affect the total

fission (σ_f or MT18 according to ENDF-6 format [27]) and radiative capture (σ_γ or MT102) microscopic cross sections of the main fissile nuclides composing the fuel elements of the reactor. The nuclides and their atomic densities are reported in table 2.

Table 2: Nuclides considered for the GPT UQ study.

Nuclide	Inner fuel mass fraction %	Outer fuel mass fraction %
U-234	$2.07419 \cdot 10^{-3}$	$1.91216 \cdot 10^{-3}$
U-235	$2.79419 \cdot 10^{-1}$	$2.57515 \cdot 10^{-1}$
U-236	$6.91511 \cdot 10^{-3}$	$6.37300 \cdot 10^{-3}$
U-238	$6.88468 \cdot 10^{+1}$	$6.34847 \cdot 10^{+1}$
Pu-238	$4.41008 \cdot 10^{-1}$	$5.64897 \cdot 10^{-1}$
Pu-239	$1.07564 \cdot 10^{+1}$	$1.37778 \cdot 10^{+1}$
Pu-240	$5.10655 \cdot 10^{+0}$	$6.53959 \cdot 10^{+0}$
Pu-241	$1.15483 \cdot 10^{+0}$	$1.47901 \cdot 10^{+0}$
Pu-242	$1.45497 \cdot 10^{+0}$	$1.86386 \cdot 10^{+0}$
Am-241	$2.47320 \cdot 10^{-1}$	$3.16741 \cdot 10^{-1}$

Figure 3 shows an example of the typical behaviour of the six-group macroscopic cross section relative sensitivity, scored on the ECCO 33-group structure for Pu-239 with a perturbation in the MT18 reaction. As one may expect from physical intuition, the sensitivity per unit lethargy is very large for the sub-groups belonging to the coarse group where the cross section is collapsed, while it is negligible for the other sub-groups, with the relevant exception of the thermal region. In these cases, it is interesting to notice that both $\Sigma_{f,5}$ and $\Sigma_{f,6}$ are sensitive to perturbations occurring at higher energies sub-groups outside the coarse groups within the thermal range.

The energy behaviour of the sensitivity profiles can be explained referring to the different rôle played by the direct and indirect terms appearing in eq. (5). In the fast and intermediate groups the direct sensitivity dominates the overall sensitivity behaviour, while in the lowest-energy groups the indirect contribution from higher energies is non-negligible. These graphs also report the relative variance extracted from the covariance matrix evaluated on the same 33-group grid, allowing to highlight by simple inspection that there are cases in which the largest sensitivity corresponds to the lowest uncertainty in the nuclear data.

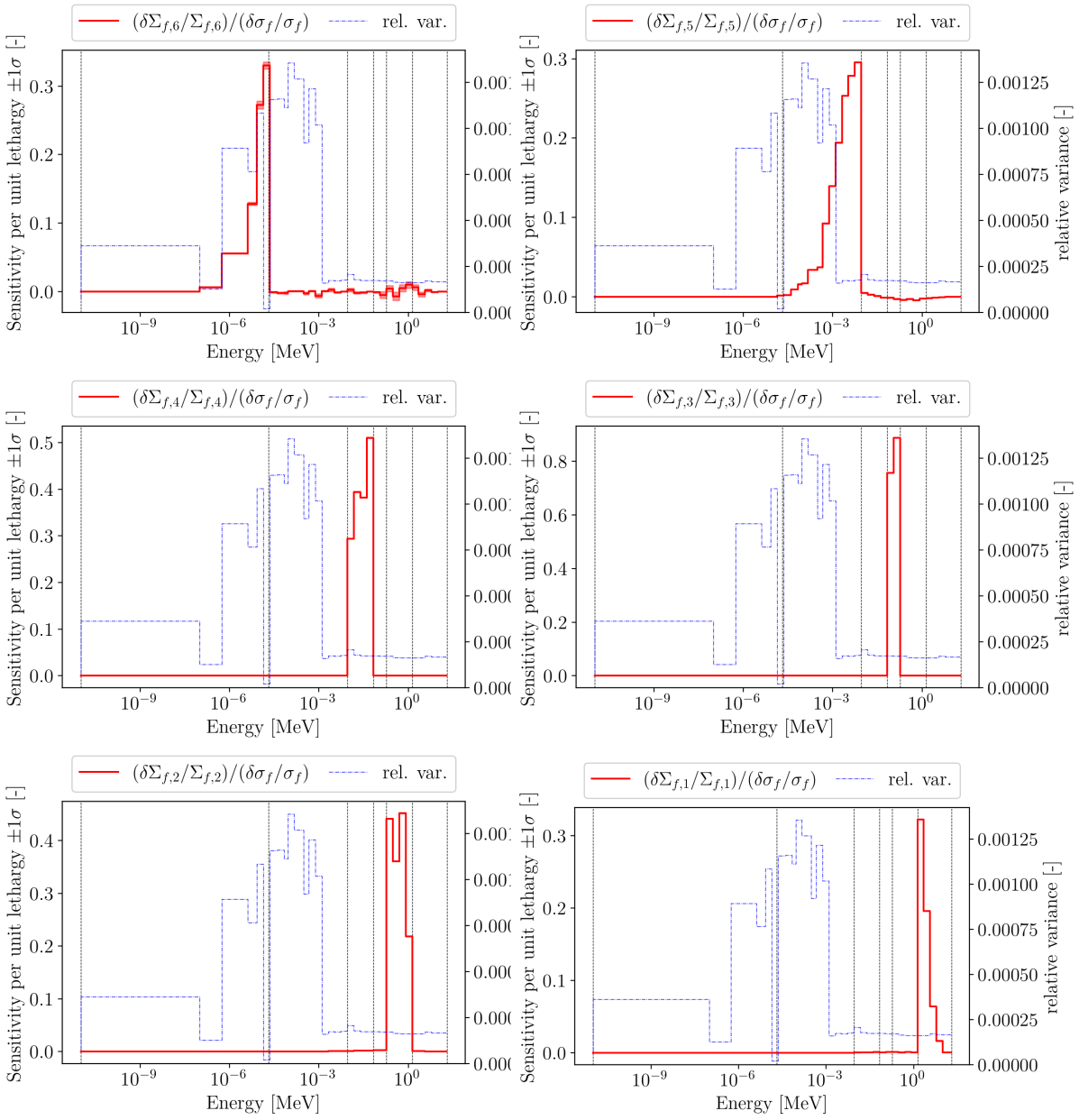

Figure 3: Sensitivity coefficients with respect to the total fission microscopic cross section (MT18) of Pu-239 for $\Sigma_{f,g}$, scored on ECCO 33-group structure with GPT.

It should be remarked that, in spite of its limitations, GPT still is the best choice for the purpose of sensitivity analysis, since it allows a straightforward physical interpretation to the energy-dependent sensitivities. On the contrary, the energy-integrated projected sensitivities provided by XGPT do not have a physically intuitive interpretation.

The sensitivity coefficients have been computed simulating 10^9 active neutron histories (10^6 neutrons per generation, 10^3 generations divided in 25 batches), starting from an already converged fission source, initialised with $5 \cdot 10^8$ inactive histories. The number of neutron latent generations used for the adjoint estimator is 10, which seems an adequate number according to the convergence trends depicted in figure 4. This graph shows the uncertainties of $\Sigma_{c,1}$ and k_{eff} computed using the sensitivity coefficients evaluated with different numbers of latent generations.

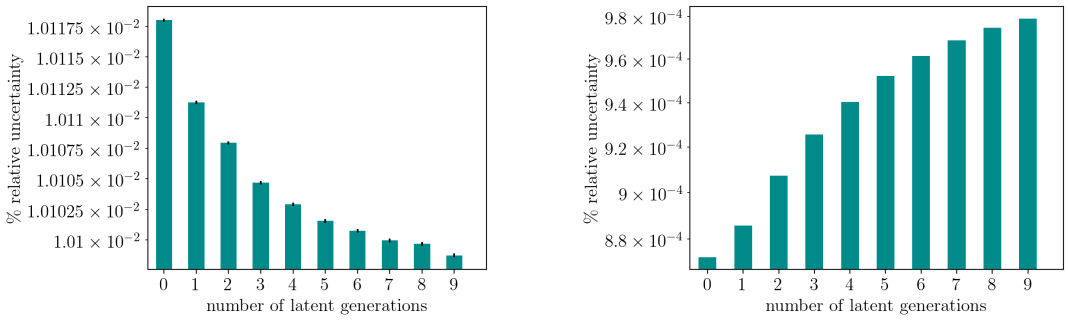

Figure 4: Latent generation convergence trend for $\Sigma_{c,1}$ (left) and k_{eff} (right). In the right plot the error bars are very small and, thus, not visible.

Figures 5 and 6 show the contribution of each actinide present in the inner and outer fuel compositions to the percentage uncertainty induced in $\Sigma_{f,g}$ and $\Sigma_{c,g}$, by the uncertainties in the MT18 and MT102 reactions. The largest contributions are due to Pu-239 and U-238, which are also the most abundant fissile and fissionable nuclides, respectively. Observing these graphs it is also possible to conclude that the uncertainties in the two fuel regions are very similar, in spite of the slightly different compositions and flux spectra.

3.2. Comparison between XGPT and GPT results

In this section a comparison between the uncertainty estimated with the GPT and XGPT methods is carried out, in order to better highlight their different features in the framework of the Monte Carlo method. The comparison

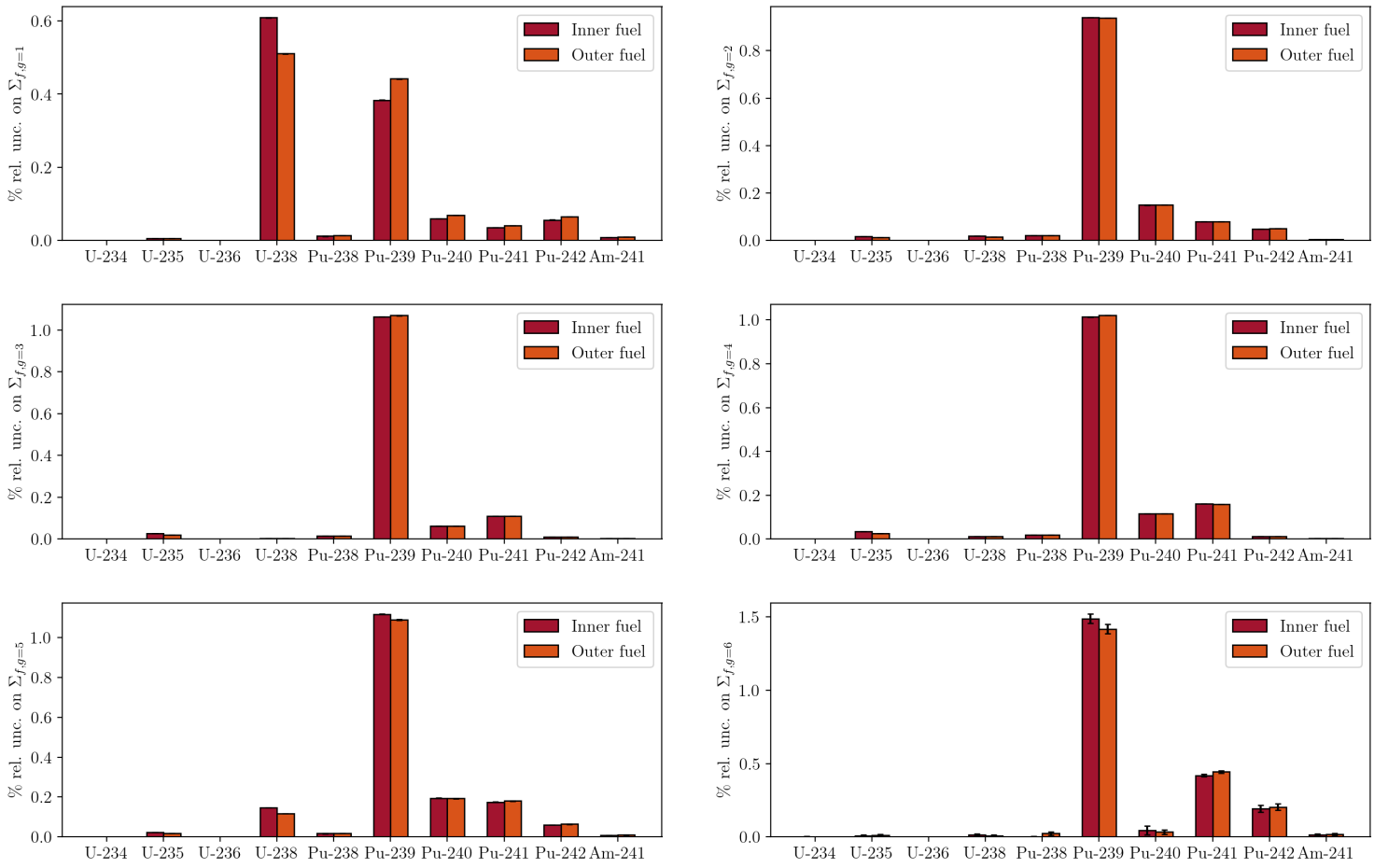

Figure 5: Nuclide contributions to the total % uncertainty on $\Sigma_{f,g}$ homogenised over the inner and outer fuel regions. The first group (the fastest) is on top-left, the sixth is on bottom-right.

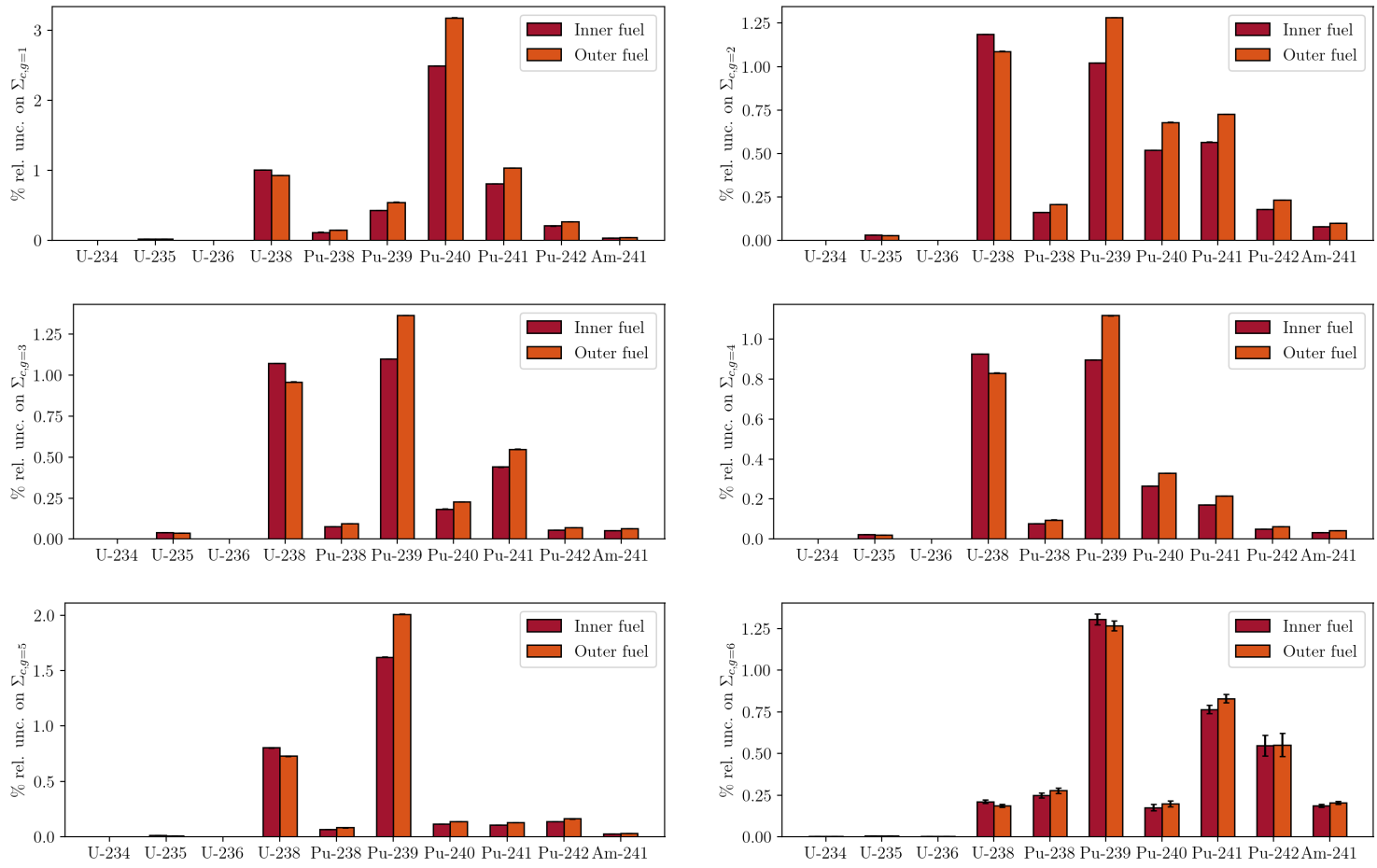

Figure 6: Nuclide contributions to the total % uncertainty on $\Sigma_{c,g}$ homogenised over the inner and outer fuel regions. The first group (the fastest) is on top-left, the sixth is on bottom-right.

is performed focusing on the impact of two specific isotopes, namely Pu-239 and U-238, on k_{eff} and on the six-group capture and fission cross sections homogenised over the inner fuel region of the ALFRED reactor. The motivation of the isotopes choice is two-fold. Firstly, they are the most relevant from the uncertainty point of view, as concluded in section 3.1. Secondly, their covariance matrices have different features that evidence the impact of the POD-SVD truncation error on the final calculation results. To the authors' knowledge, this is the first application of XGPT for the propagation of the nuclear data uncertainty throughout the overall homogenisation and collapsing procedure.

In order to analyse the impact of the different energy discretisations on the final uncertainties, the XGPT calculations are carried out using two sets of covariances. The first one is computed on the ECCO 33-group grid, the same employed for the GPT analysis, while the second one is defined on a fine-group structure composed of 1500 groups. It has to be noticed that the current limitations in the ERRORR module of NJOY, used to process the ENDF-6 files, restricts the maximum number of groups around 1500. Consequently, the fine-group grid has been defined using the ECCO 1968-group as a starting point and the 1500 groups have been distributed in order to cover the energy range consistently, also considering the flux spectra of the fuel regions and of the radial and axial reflectors, reported in figure 7. Due to the poor statistics in the lower and upper energy range limits, which is a consequence of the physics of LFRs, most of the bins have been distributed in the epithermal region. The details of the fine-group structure are reported in table 3, while figure 8 shows a graphical representation of the 6, 33 and 1500-group grids employed in this paper. The direct inspection of figure 9

Table 3: Energy groups specifications to construct the 1500-group grid employed for the calculations.

Region	Lower boundary [MeV]	Upper boundary [MeV]	Points in lethargy
Thermal 1	10^{-11}	10^{-7}	1
Thermal 2	10^{-7}	10^{-5}	20
Epithermal	10^{-5}	10^{1}	1472
Fast	10^{1}	$2 \cdot 10^{1}$	10

shows the typical decay of the singular values extracted from the covariance matrices processed on the 33-group and the 1500-group structures. In the

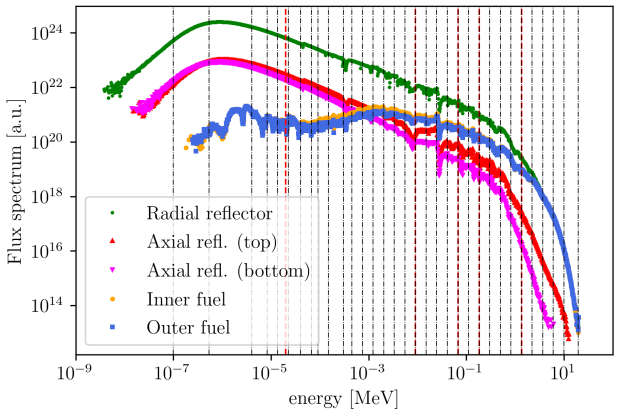

Figure 7: Inner fuel, outer fuel and radial reflector (dummy element) flux spectra. The red dashed line represent the six-energy groups while the black dashed-dotted lines identify the ECCO 33-group grid.

first case, a similar amount of basis functions, 56 and 65, is needed to approximate the Pu-239 and U-238 covariances, respectively, to the prescribed tolerance ($1-\mathcal{E} \leq 10^{-8}$). When the covariances are processed on 1500 groups, 191 and 1446 basis functions are needed for U-238 and Pu-239, respectively. The large difference between the number of basis functions required by each isotope covariance in the two cases can be better understood looking at the associated correlation matrices presented in figure 1. In the U-238 case the 1500-group description does not add significant changes to the correlation matrices appearance, while the higher resolution in the fast and intermediate regions is evident for the Pu-239 case. Figure 10 shows the impact of the covariance truncation error on the final uncertainty estimated with eq. (17). Even in the worst case scenario, represented by the Pu-239 MT18 uncertainty on $\Sigma_{f,2}$, a number of basis functions around 200 yields a truncation error that is far below the statistical one. This behaviour justifies the adoption of the POD reduction technique, proving that even tolerances larger than the one initially adopted are here acceptable.

It is clear that the number of energy points used to score the sensitivity profiles should match the rank of the covariance matrix in eq. (1). Therefore, in the case a continuous-energy (i.e. an ultra-fine group) covariance were available, the sensitivities should be computed on the same grid. Obviously, this would not be affordable, neither by a deterministic nor by a stochastic code, because of the too demanding computational burden. On the contrary,

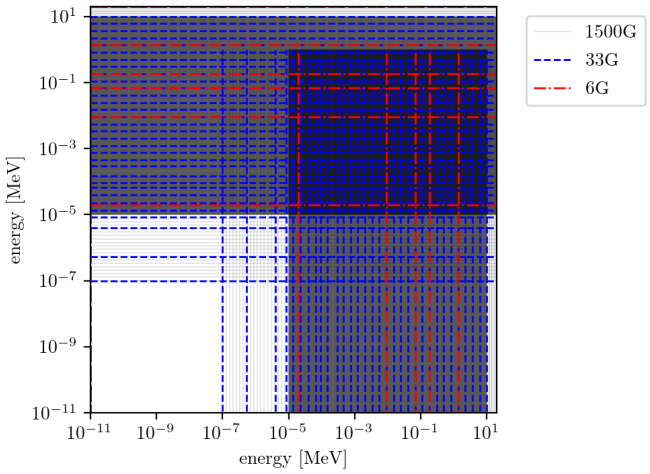

Figure 8: Energy group structures employed for the sensitivity and uncertainty analyses.

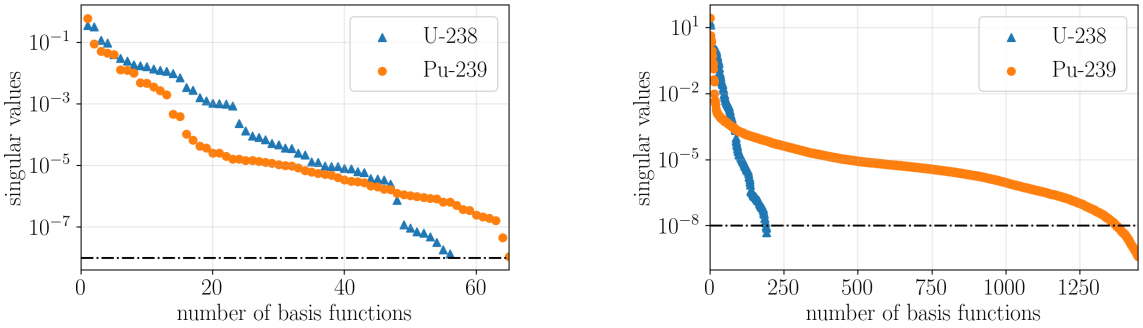

Figure 9: POD eigenvalues decay for the covariance matrices of Pu-239 and U-238 evaluated on ECCO 33-group (left) and on the 1500-group energy structures (right). The dashed-dotted black line represents the tolerance level.

if eq. (17) were employed, a reduced number of energy-integrated projected sensitivities would be needed, as the POD basis dimension t is usually much smaller than the covariance rank m, due to the fast singular values decay. This fact implies that there is no limit to the energy detail considered in the sensitivity calculation, making this technique suitable for stochastic methods or asymptotic theory [28].

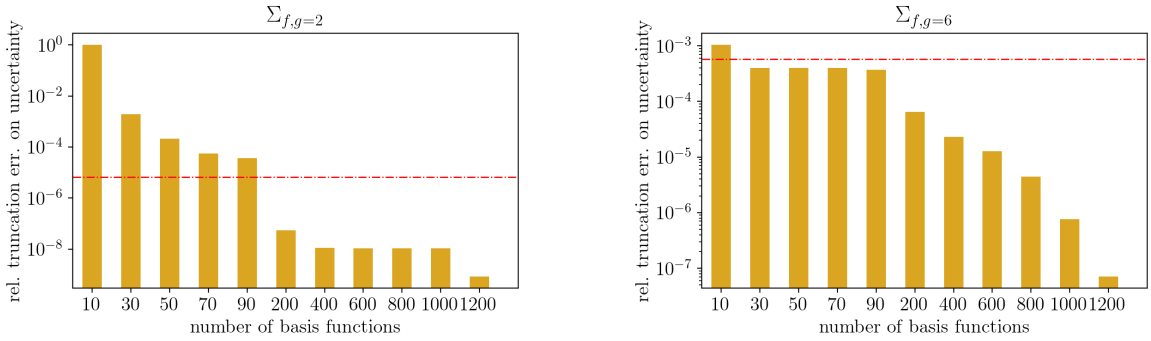

Figure 10: POD truncation error on the relative Σ_f uncertainty due to Pu-239 MT18. The statistical error is represented by the dashed-dotted red line.

Tables 4 through 7 show the group-wise percentage uncertainty on the capture and fission homogenised cross sections due to the uncertainty of U-238 and Pu-239 MT18 and MT102. All the results are presented with their statistical uncertainty, propagated through eq. (17) using classical linear uncertainty propagation and neglecting the cross-correlation among the terms. Tables 4 and 5 present the results computed on the 33-group grid with GPT and XGPT, respectively. The overall agreement between the results is accept-

Table 4: Percentage uncertainties evaluated scoring both the GPT sensitivities and the covariances on the 33-group structure.

g	U-238				Pu-239			
	σ_f (MT18)		σ_c (MT102)		σ_f (MT18)		σ_c (MT102)	
	Σ_f	Σ_c	Σ_f	Σ_c	Σ_f	Σ_c	Σ_f	Σ_c
1	0.60903(39)	0.00460(24)	0.00225(42)	1.00988(81)	0.38327(79)	0.0220(14)	0.00270(95)	0.42913(68)
2	0.01813(13)	0.000161(94)	0.00414(18)	1.18629(27)	0.93934(38)	0.00658(29)	0.00659(43)	1.02227(29)
3	0.003286(33)	0.00024(13)	0.00240(20)	1.07346(27)	1.06370(41)	0.00557(36)	0.00242(35)	1.10009(38)
4	0.001834(20)	0.00097(17)	0.01290(17)	0.92626(34)	1.01347(39)	0.02507(42)	0.01231(38)	0.89525(54)
5	0.00557(33)	0.00246(39)	0.14641(67)	0.80428(92)	1.1121(16)	0.15478(96)	0.3103(18)	1.6214(22)
6	0.0055(42)	0.0055(43)	0.0149(67)	0.2118(99)	1.279(28)	0.103(17)	0.740(43)	1.297(33)

able within the statistical confidence interval, with some relevant exceptions,

e.g. for the U-238 MT102 uncertainty on Σ_c. These discrepancies can be

Table 5: Percentage uncertainties evaluated scoring both the XGPT sensitivities and the covariances on the 33-group structure.

g	U-238				Pu-239			
	σ_f (MT18)		σ_c (MT102)		σ_f (MT18)		σ_c (MT102)	
	Σ_f	Σ_c	Σ_f	Σ_c	Σ_f	Σ_c	Σ_f	Σ_c
1	0.83637(95)	0.00433(41)	0.00288(38)	2.1566(17)	0.7045(10)	0.0203(13)	0.00299(82)	1.0935(13)
2	0.003942(86)	0.00015(11)	0.00348(10)	0.87510(67)	0.68924(63)	0.00687(27)	0.00654(35)	0.87966(48)
3	0.002744(17)	0.00011(13)	0.00243(21)	1.6049(12)	1.2850(11)	0.00553(42)	0.00257(37)	1.7165(12)
4	0.0013672(59)	0.00094(16)	0.01136(20)	1.14865(41)	0.82977(69)	0.02489(43)	0.01207(34)	1.07996(65)
5	0.00725(22)	0.00246(37)	0.14365(66)	0.52445(91)	1.4452(28)	0.13179(90)	0.2971(20)	0.9774(20)
6	0.0064(82)	0.0117(77)	0.015(11)	0.156(11)	0.393(28)	0.097(21)	0.555(32)	0.441(32)

explained recalling eq. (13), where an approximation is introduced to evaluate the direct projected sensitivity. The integration error is reduced when both the direct sensitivities and the basis functions are estimated on the 1500-group grid, yielding an overall good agreement, at least in the statistical sense (see table 6). If Serpent 2 would estimate also the direct sensitivity inside the transport process, the two methods should produce a set of statistically equivalent results, since the same multi-group structure is employed. It should be remarked here that columns Σ_c for MT18 and Σ_f for MT102 are identical in tables 6 and 5 for both species, as the direct effect is exactly zero.

Table 6: Percentage uncertainties evaluated with XGPT scoring the indirect sensitivities on the 33-group structure and the direct effect (including the basis functions) on the 1500-group structure.

g	U-238				Pu-239			
	σ_f (MT18)		σ_c (MT102)		σ_f (MT18)		σ_c (MT102)	
	Σ_f	Σ_c	Σ_f	Σ_c	Σ_f	Σ_c	Σ_f	Σ_c
1	0.60075(62)	0.00433(41)	0.00288(38)	0.65441(87)	0.38291(79)	0.0203(13)	0.00299(82)	0.3229(10)
2	0.026123(90)	0.00015(11)	0.00348(10)	0.79698(47)	0.67001(51)	0.00687(27)	0.00654(35)	0.54147(31)
3	0.004379(12)	0.00011(13)	0.00243(21)	1.47092(83)	1.6264(10)	0.00553(42)	0.00257(37)	1.62678(95)
4	0.0016899(69)	0.00094(16)	0.01136(20)	1.15964(35)	1.01185(74)	0.02489(43)	0.01207(34)	1.05397(60)
5	0.00508(28)	0.00246(37)	0.14365(66)	0.63134(82)	1.5018(22)	0.13179(90)	0.2971(20)	1.0821(20)
6	0.0064(82)	0.0117(77)	0.015(11)	0.396(12)	1.191(38)	0.097(21)	0.555(32)	1.069(37)

Table 7 shows the results of the XGPT calculations where both direct and indirect sensitivities are scored on the 1500-group grid. These results have to be considered as the reference, since they are scored on the finest energy grid. Their agreement with the GPT case is very good, except for the impact of Pu-239 MT18 on $\Sigma_{f,6}$ and $\Sigma_{c,6}$, where GPT gives underestimated results.

Table 7: Percentage uncertainties evaluated scoring both the XGPT sensitivities and the covariances on the 1500-group structure.

g	U-238				Pu-239			
	σ_f (MT18)		σ_c (MT102)		σ_f (MT18)		σ_c (MT102)	
	Σ_f	Σ_c	Σ_f	Σ_c	Σ_f	Σ_c	Σ_f	Σ_c
1	0.61121(54)	0.00494(17)	0.00230(40)	0.95971(69)	0.38295(86)	0.0216(13)	0.00399(80)	0.42283(95)
2	0.01783(10)	0.000224(70)	0.00440(13)	1.18858(63)	0.94018(65)	0.00666(26)	0.00682(38)	1.02393(41)
3	0.003328(27)	0.000057(30)	0.00251(23)	1.07471(59)	1.06230(74)	0.00533(41)	0.00228(39)	1.09587(82)
4	0.001930(16)	0.00098(14)	0.01188(18)	0.91814(43)	1.00993(71)	0.02518(43)	0.01190(38)	0.89899(61)
5	0.00609(26)	0.00276(26)	0.14526(72)	0.80626(88)	1.0021(19)	0.14730(95)	0.2197(17)	1.6575(20)
6	0.0059(68)	0.0040(36)	0.0126(48)	0.202(16)	2.121(57)	0.075(27)	0.646(47)	1.240(47)

This difference is remarkable, and is due to the larger number of low-energy groups employed in the 1500-group grid (XGPT) with respect to the ECCO 33-group grid (GPT), as it can be noticed in figure 8. On the contrary, table 8

Table 8: k_{eff} relative uncertainty in *pcm*.

Nuclide	GPT 33	XGPT 33	XGPT 1500
U-238	101.55(11)	99.66(11)	101.53(12)
Pu-239	259.61(23)	259.63(23)	259.18(34)

shows that the total uncertainty due to MT18 and MT102 on k_{eff} computed with GPT and XGPT using the two grids yield very similar results. This agreement is a consequence of the absence of direct contributions, which may introduce large discrepancies between GPT and XGPT, and of the integral nature of the effective multiplication parameter, which is less sensitive to the energy discretisation employed in the calculation.

The evidences observed in this section have two important implications: *i*) from the methodological point of view, it is proven that XGPT allows a higher energy resolution compared to Monte Carlo GPT, and this higher precision do have indeed a non-negligible effect when the responses are not integrated on the whole energy range *ii*) from the physical point of view, it is of paramount importance to use an adequate number of low-energy groups even in the case of a fast system analysis.

3.3. Multi-group constant distributions

The first-order model described by eq. (19) is applied to sample the output responses of interest, e.g. the multi-group fission and capture cross

sections homogenised over the inner fuel region. Figure 11 shows the best-estimate and perturbed fission and capture cross sections for Pu-239, sampled according to the covariance matrix scored on the 1500-group grid, while figure 12 shows the best-estimate homogenised and collapsed cross sections and their uncertainties. These graphs should help the reader to visualise how

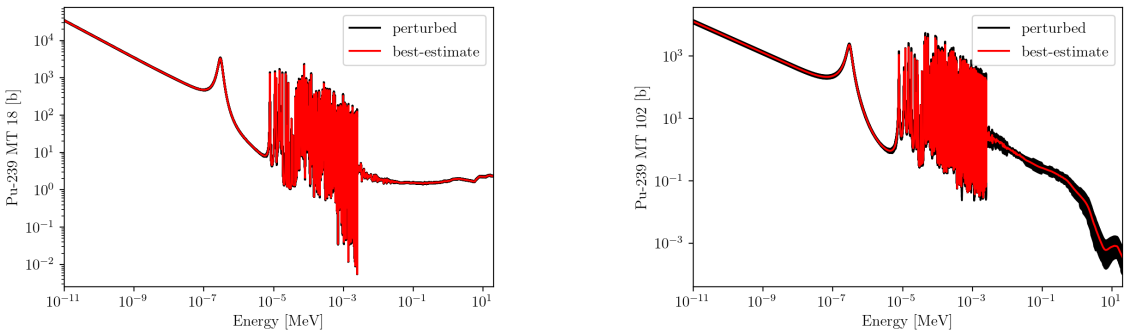

Figure 11: Best-estimate and set of perturbed MT18 (left) and MT102 (right) cross sections for Pu-239. The black band is obtained by superposition of 100 perturbed values.

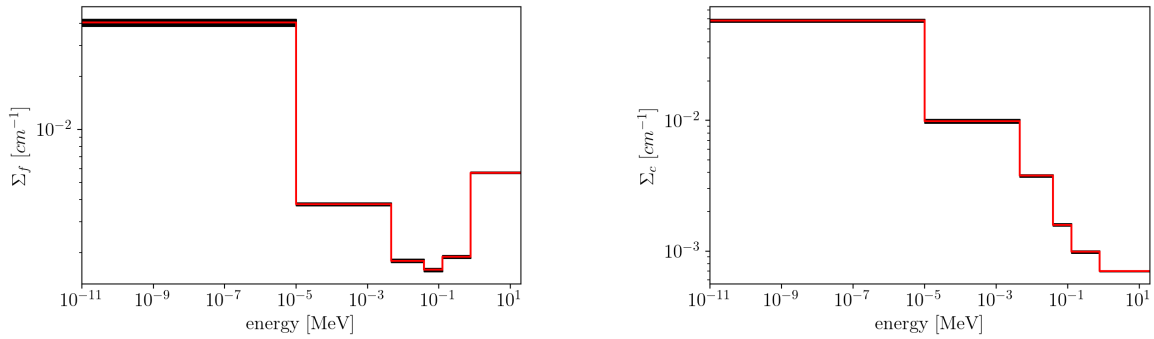

Figure 12: Best-estimate (red) and 2-σ uncertainty (black) on 6-group values of fission (left) and capture (right) cross sections for Pu-239.

the uncertainty in the raw nuclear data is propagated to the multi-group cross sections through the homogenisation and collapsing procedure. Since the raw nuclear data perturbations have been sampled assuming a multi-variate normal distribution, also the final output are normally distributed,

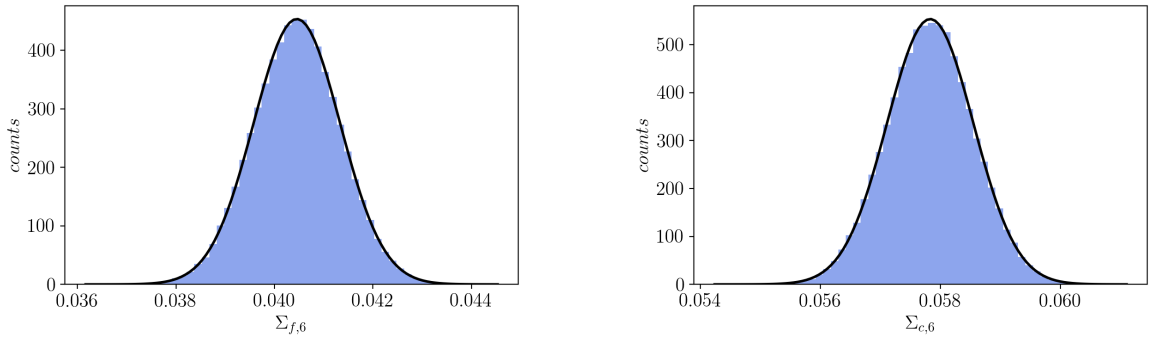

Figure 13: Sample distributions for $\Sigma_{f,6}$ (left) and $\Sigma_{c,6}$ (right) due to the uncertainty in Pu-239 MT18 and MT102. The histograms have been constructed with 10^5 samples. The superimposed black line follows the Gaussian function.

as visible in figure 13. For sake of conciseness, only the group featured by the largest uncertainty is reported for both responses. The standard deviations associated to the distributions shown are consistent with the ones presented in table 7.

Finally, figure 14 reports the structure of the correlation matrices for the input raw nuclear data, scored on the 1500-group grid, and of the Serpent 2 homogenised and collapsed cross sections, evaluated on the 6-group grid. The output correlation matrix has been estimated with 10^5 samples, generated with eq. (19).

4. Conclusions

In this paper, an assessment of the GPT and XGPT methods implemented in the Serpent 2 Monte Carlo code is carried out. The attention is focused on the uncertainty propagation from the raw nuclear data to the energy collapsed and spatially homogenised cross sections for the ALFRED reactor design.

In the first part of the paper, the main differences between the two methods are discussed and the calculation steps needed to estimate the direct sensitivity contributions in the case of a linear reaction rate response are outlined. Both GPT and XGPT allow to score first-order estimates of the sensitivity coefficients, which are then employed in the sandwich rule to compute the response variance. The most relevant difference between the two

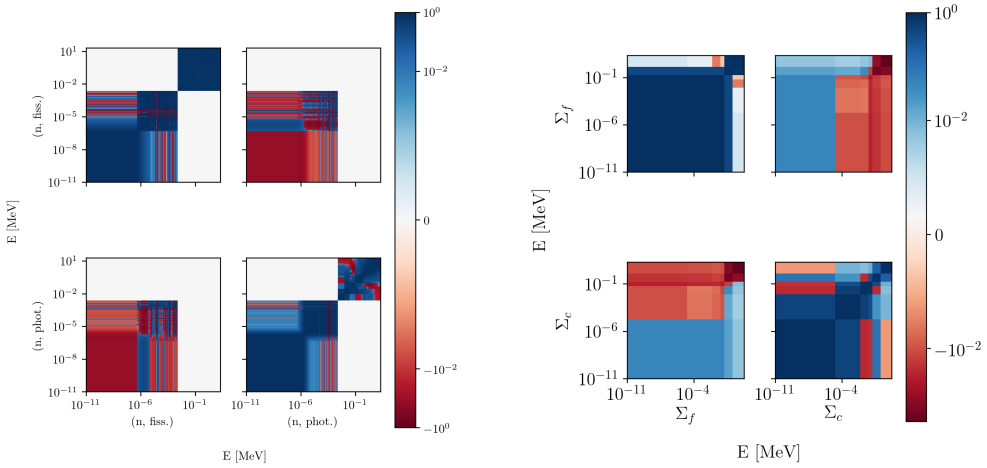

Figure 14: Structure of the correlation matrices for the Pu-239 raw nuclear data scored on the 1500-group grid (left) and for the collapsed and homogenised cross section of the inner fuel region (right). The energy range is the same for all graphs.

methods lies within the energy treatment: XGPT is an inherently continuous-energy approach, whilst GPT requires the multi-group approximation.

Afterwards, GPT is adopted to carry out an uncertainty quantification study involving all the heavy nuclides present in the inner and outer fuel compositions of the ALFRED reactor core. This study has shown that the two most abundant nuclides, i.e. Pu-239 and U-238, are the top contributors to the overall uncertainty on the few-group cross sections Σ_f and Σ_c for both the regions considered in the homogenisation process, i.e. the inner and outer fuel assemblies.

The second part of the paper is devoted to compare the uncertainties on Σ_f, Σ_c and k_{eff} obtained previously with GPT to the ones provided by XGPT, focusing on the impact of the different energy structures employed to score the sensitivities. The major outcome of this comparison is that a more precise energy resolution can be achieved using the XGPT method, making it the preferable choice among the perturbative methods for uncertainty and sensitivity analyses in a Monte Carlo framework, due to its continuous-energy feature. However, according to the specific system (e.g., a thermal reactor) and to its output responses of interest, the use of a coarse-group GPT approach could be sufficient if only a rough estimate of the uncertainty is required or if the energy effects are less relevant. In order to draw some general conclusions, different systems and responses should be compared in

future works.

Moreover, this comparison has also shown that the adoption of an adequate number of low-energy groups is of paramount importance even in the case of a fast system analysis. At last, the output correlation matrix for the output responses Σ_f and Σ_c is compared to the correlation matrix of the input Pu-239 nuclear data considered in the paper.

As a further development to this activity, it would be extremely interesting to analyse the impact on XGPT calculations due to the adoption of fine-group covariances, available in the legacy ENDF-6 format, and continuous-energy covariances extracted from a set of random evaluations, e.g. performed with the T6 package. Such an analysis would shed some light on the influence of the input parameter distributions on the final output and could highlight the importance for pointwise covariances with respect to fine-group ones.

Data availability

The complete datasets and scripts employed to pre- and post-process the Serpent calculations presented in this paper are available in the open access Zenodo repository 10.5281/zenodo.4540785.

Acknowledgments

Computational resources were provided by HPC@POLITO, a project of Academic Computing within the Department of Control and Computer Engineering at Politecnico di Torino (http://www.hpc.polito.it).

The authors would like to thank Ville Valtavirta for his guidance through the XGPT implementation in the Serpent 2 code.

References

[1] H. Glaeser. Evaluation of licensing margins of reactors using "best estimate" methods including uncertainty analysis. In *IAEA Regional Workshop on Application of Deterministic Best Estimate (BE) Safety Analysis for Advanced NPP, AERB of India, Mumbai*, pages 13 – 17, 2010.

[2] F. D'Auria, C. Camargo, and O. Mazzantini. The best estimate plus uncertainty (BEPU) approach in licensing of current nuclear reactors. *Nuclear Engineering and Design*, 248:317 – 328, 2012.

[3] E. Hüllermeier and W. Waegeman. Aleatoric and epistemic uncertainty in machine learning: a tutorial introduction. *CoRR*, 2019.

[4] G. Rimpault, D. Plisson, J. Tommasi, R. Jacqmin, D. Verrier, and D. Biron. The ERANOS Code and Data System for Fast Reactor Neutronic Analyses. In *Proceedings of the PHYSOR conference 2002*, 2002.

[5] J. Leppänen, M. Pusa, and E. Fridman. Overview of methodology for spatial homogenization in the Serpent 2 Monte Carlo code. *Annals of Nuclear Energy*, 96:126–136, 2016.

[6] D. G Cacuci. *Sensitivity & Uncertainty Analysis, Volume I: Theory*. Chapman & Hall/CRC, New York, 2003.

[7] A. Gandini, M. Salvatores, and I. Dal Bono. Sensitivity study of fast reactors using generalized perturbation techniques. In *Fast Reactor Physics Vol. I. Proceedings of a Symposium on Fast Reactor Physics and Related Safety Problems*, 1968.

[8] A. Gandini and M. Salvatores. Effects of Plutonium-239 Alpha uncertainties on some significant integral quantities of fast reactors. *Nuclear Science and Engineering*, 41(3):452–455, 1970.

[9] D. Rochman, A. J. Koning, S. C. Van Der Marck, A. Hogenbirk, and C. M. Sciolla. Nuclear data uncertainty propagation: Perturbation vs. Monte Carlo. *Annals of Nuclear Energy*, 38(5):942–952, 2011.

[10] R. Bellman. *Dynamic Programming*. Rand Corporation research study. Princeton University Press, 1957.

[11] M. Aufiero, M. Martin, and M. Fratoni. XGPT: Extending Monte Carlo Generalized Perturbation Theory capabilities to continuous-energy sensitivity functions. *Annals of Nuclear Energy*, 96:295–306, 2016.

[12] J. Leppänen, M. Pusa, T. Viitanen, V. Valtavirta, and T. Kaltiaisenaho. The Serpent Monte Carlo code: Status, development and applications in 2013. *Annals of Nuclear Energy*, 82:142–150, 2015.

[13] M. Santanoceto, M. Tiberga, Z. Perkó, S. Dulla, and D. Lathouwers. Uncertainty quantification in steady state simulations of a molten salt system using polynomial chaos expansion analysis. In *Proceedings of PHYSOR Conference 2020*, 2020.

[14] G. Grasso, C. Petrovich, D. Mattioli, C. Artioli, P. Sciora, D. Gugiu, G. Bandini, E. Bubelis, and K. Mikityuk. The core design of ALFRED, a demonstrator for the European lead-cooled reactors. *Nuclear Engineering and Design*, 278:287–301, 2014.

[15] R. E. MacFarlane, D. W. Muir, R. M. Boicourt, A. C. Kahler, J. L. Conlin, and W. Haeck. The NJOY Nuclear Data Processing System, Version 2016 (LA-UR–17-20093). Technical report, 2018.

[16] D. Pelowitz, T. Goorley, M. James, Thomas Booth, F. Brown, J. Bull, Lawrence Cox, J. Durkee, J. Elson, Michael Fensin, R. Forster, J. Hendricks, H. Hughes, Russell Johns, B. Kiedrowski, Roger Martz, S. Mashnik, Gregg Mckinney, R. Prael, and T. Zukaitis. MCNP6 user's manual, 05 2013.

[17] A.J. Koning and D. Rochman. Modern nuclear data evaluation with the TALYS code system. *Nuclear Data Sheets*, 113(12), 12 2012.

[18] A.J. Koning, D. Rochman, J.-Ch. Sublet, N. Dzysiuk, M. Fleming, and S. van der Marck. TENDL: Complete nuclear data library for innovative nuclear science and technology. *Nuclear Data Sheets*, 155:1 – 55, 2019. Special Issue on Nuclear Reaction Data.

[19] A.J. Koning. Tools for TALYS: Autotalys, T6, TENDL, libraries and more. Technical report, 2020.

[20] D.A. Brown, M.B. Chadwick, R. Capote, A.C. Kahler, A. Trkov, M.W. Herman, A.A. Sonzogni, Y. Danon, A.D. Carlson, M. Dunn, D.L. Smith, G.M. Hale, G. Arbanas, R. Arcilla, C.R. Bates, B. Beck, B. Becker, F. Brown, R.J. Casperson, J. Conlin, D.E. Cullen, M.-A. Descalle, R. Firestone, T. Gaines, K.H. Guber, A.I. Hawari, J. Holmes, T.D. Johnson, T. Kawano, B.C. Kiedrowski, A.J. Koning, S. Kopecky, L. Leal, J.P. Lestone, C. Lubitz, J.I. Márquez Damián, C.M. Mattoon, E.A. McCutchan, S. Mughabghab, P. Navratil, D. Neudecker, G.P.A. Nobre, G. Noguere, M. Paris, M.T. Pigni, A.J. Plompen, B. Pritychenko, V.G. Pronyaev, D. Roubtsov, D. Rochman, P. Romano, P. Schillebeeckx, S. Simakov, M. Sin, I. Sirakov, B. Sleaford, V. Sobes, E.S. Soukhovitskii, I. Stetcu, P. Talou, I. Thompson, S. van der Marck, L. Welser-Sherrill, D. Wiarda, M. White, J.L. Wormald, R.Q. Wright, M. Zerkle, G. Žerovnik, and Y. Zhu. ENDF/B-VIII.0: The 8th major release of the nuclear reaction data library with CIELO-project cross sections, new standards and thermal scattering data. *Nuclear Data Sheets*, 148:1 – 142, 2018. Special Issue on Nuclear Reaction Data.

[21] A. E. Johnson, D. Kotlyar, S. Terlizzi, and G. Ridley. serpentTools: A Python package for expediting analysis with Serpent. *Nuclear Science and Engineering*, 194(11):1016–1024, 2020.

[22] S. Volkwein. Model reduction using proper orthogonal decomposition. *Lecture notes, Institute of Mathematics and Scientific Computing, University of Graz. see http://www. uni-graz. at/imawww/volkwein/POD. pdf*, 1025, 2011.

[23] L. Fiorito, G. Žerovnik, A. Stankovskiy, G. Van den Eynde, and P. E. Labeau. Nuclear data uncertainty propagation to integral responses using SANDY. *Annals of Nuclear Energy*, 101:359–366, 2017.

[24] N. Abrate, M. Aufiero, S. Dulla, and L. Fiorito. Nuclear data uncertainty quantification in molten salt reactors with XGPT. In *Proceedings of the ANS International Conference M&C2019*, Portland, OR, August 25-29 2019.

[25] G. F. Nallo, N. Abrate, S. Dulla, P. Ravetto, and D. Valerio. Neutronic benchmark of the FRENETIC code for the multiphysics analysis of lead fast reactors. *The European Physical Journal Plus*, 135:238, 2020.

[26] V. Valtavirta. Nuclear data uncertainty propagation to Serpent generated group and time constants. Technical Report VTT-R-04681-18, VTT research center, Finland, 2018.

[27] M. Herman, A. Trkov, et al. ENDF-6 formats manual. Technical Report BNL-90365-2009 Rev.1, 2010.

[28] S. Dulla and P. Ravetto. A re-visitation of space asymptotic theory in neutron transport. *European Physical Journal Plus*, 135:347, 2020.